NANO · MICRO small
www.small-journal.com

Dynamic Sessile-Droplet Habitats for Controllable Cultivation of Bacterial Biofilm

*Zengjun Jin, Mengyue Nie, Ran Hu, Tianhu Zhao, Jingyue Xu, Dongwei Chen, Juanli Yun, Luyan Z. Ma, and Wenbin Du**

Bacterial biofilms play essential roles in biogeochemical cycling, degradation of environmental pollutants, infection diseases, and maintenance of host health. The lack of quantitative methods for growing and characterizing biofilms remains a major challenge in understanding biofilm development. In this study, a dynamic sessile-droplet habitat is introduced, a simple method which cultivates biofilms on micropatterns with diameters of tens to hundreds of micrometers in a microfluidic channel. Nanoliter plugs are utilized, spaced by immiscible carrier oil to initiate and support the growth of an array of biofilms, anchored on and spatially confined to the micropatterns arranged on the bottom surface of the microchannel, while planktonic or dispersal cells are flushed away by shear force of aqueous plugs. The performance of the aforementioned method of cultivating biofilms is demonstrated by *Pseudomonas aeruginosa* PAO1 and its derived mutants, and quantitative antimicrobial susceptibility testing of PAO1 biofilms. This method could significantly eliminate corner effects, avoid microchannel clogging, and constrain the growth of biofilms for long-term observations. The controllable sessile droplet-based biofilm cultivation presented in this study should shed light on more quantitative and long-term studies of biofilms, and open new avenues for investigation of biofilm attachment, growth, expansion, and eradication.

1. Introduction

Biofilms are sessile and well-organized microbial consortia that predominate in environmental, industrial, and clinical settings.[1] Biofilms exert a great impact on biogeochemical cycling,[2] wastewater processing,[3] and infectious diseases.[4] Commensal biofilms are indispensable components of healthy human microbiome.[5,6] Traditional methods to grow biofilms in vitro can be classified in two categories[7]: static cultivation or flow reactors. Under static conditions, biofilms can grow on agar plates, the surface of well plates, or the air–water interface, with few mechanical or thermal fluctuations. The major disadvantages include the lack of continuous replacement of medium and interference of planktonic cells with the sessile biofilms. Flow reactors were advanced with continuous supply of fresh medium and stimulants, incorporation of shear forces to mimic natural conditions, access of microscopic imaging of the biofilms. Microfluidic flow cells have been introduced to further reduce reagent consumption and provide more precise hydrodynamic and chemical microenvironments.[8–14] However, potential drawbacks to microfluidic flow cells include limited periods of observation,[15] unpredictable changes of the hydrodynamic environment due to overgrowth of biofilms,[16] development of biofilm gradients from the inlet of the device to the outlet,[17] corner effects in rectangular channels,[18] and decreased consistency of biofilm growth between experimental batches. Due to the inherent complexity and heterogeneity of biofilms, new tools and technologies are urgently warranted for more quantitative study of biofilms, including their development, structure, and biofilm–drug interaction.

Here we demonstrated a novel method for cultivation of bacterial biofilms in sessile droplets, which were named as the dynamic sessile-droplet habitat (DSH). The method is constructed based on droplet microfluidic technique.[19] Arrays of sessile droplets attached on the bottom surface of the microchannel were designed for seeding bacterial cells and providing space and nutrients for growth of biofilms spatially constrained to them. Nanoliter plugs flowing through the microchannel could dynamically exchange with the sessile droplets to support long-term growth of the biofilms and stimulate the biofilms with shear stress. We analyzed the growth of biofilms of *Pseudomonas aeruginosa* PAO1 and its mutants, demonstrating the considerable potential of this novel method in cultivation and characterization of microbial biofilms.

Z. J. Jin, M. Y. Nie, R. Hu, T. H. Zhao, J. Y. Xu,
Dr. D. W. Chen, Dr. J. L. Yun, Prof. L. Z. Ma, Prof. W. B. Du
State Key Laboratory of Microbial Resources
Institute of Microbiology
Chinese Academy of Sciences
Beijing 100101, China
E-mail: wenbin@im.ac.cn
Z. J. Jin, M. Y. Nie, T. H. Zhao, J. Y. Xu
College of Life Sciences
University of the Chinese Academy of Sciences
Beijing 100049, China
R. Hu, Prof. L. Z. Ma, Prof. W. B. Du
Savaid Medical School
University of the Chinese Academy of Sciences
Beijing 100049, China
The ORCID identification number(s) for the author(s) of this article can be found under https://doi.org/10.1002/smll.201800658.

DOI: 10.1002/smll.201800658

2. Results

2.1. Design of the Biofilm Cultivation System

To culture biofilms in precisely confined conditions with constant hydrodynamic conditions during a long time period, we followed several criteria to design the microfluidic system: i the size and shape of biofilms should be precisely controlled during growth; ii the device should permit continuous supplement of culture media; iii the device should allow appliance of controllable and predictable hydrodynamic condition to the biofilms; iv the biofilms should harbor distinct boundary for studying the expansion or dispersal behaviors. To fulfill these criteria, we introduced the DSH method based on droplet microfluidic technologies.[19–21] The device consisted of a top polydimethylsiloxane (PDMS) layer with microchannel and a bottom glass plate with arrays of hydrophilic micropatterns of different sizes (**Figure 1**A). The PDMS layer and the glass plate were aligned and put together based on reversible sealing which was waterproof and could withstand pressure lower than 35 kPa as previously reported.[22] The glass surface under the microchannel was rendered hydrophobic by silanization except the circular micropatterns. The hydrophobic PDMS microchannel rendered the generation of nanoliter aqueous plugs and subsequent flow through the channel without residues on the surface (Video S1, Supporting Information). This hydrophilic/hydrophobic hybrid patterning resulted in the formation of an array of discrete sessile droplets in the channel when aqueous plugs continuously flow through, and dynamic exchanging of the sessile droplets with the plugs due to surface tension and spatial confinement. (Figure 1D; and Video S2, Supporting Information).

To grow biofilms spatially confined in the sessile droplets, we first generated plugs with PAO1 cells using T-junction, and flowed the plugs through the channel to seed cells on the hydrophilic micropatterns (Figure 1B). The inoculation process was conducted continuously for 0.5–2 h, which ensured the irreversible attachment of several cells to each micropattern. Then, PAO1 cells flow was stopped, and culture media was infused through the channel to ensure the growth of biofilms (Figure 1C; and Video S3, Supporting Information). We monitored the dynamic development of biofilms by automated time-lapse imaging on an inverted microscope with a motorized X-Y stage. The inlets of PAO1 and culture media were physically separated by continuous oil phase. Therefore, contamination of media by bacteria during long-term cultivation was effectively avoided. Moreover, multiple inlets can be used to introduce different stimulant substances for applications such as live/dead staining (Figure S3, Supporting Information) and antimicrobial susceptibility testing (Figure 6).

2.2. Comparison of the DSH with Microfluidic Flow Cell

The biofilm growth in DSHs was compared with continuous flow cell method in terms of spatial structure, biomass, and uniformity of coverage. As shown in **Figure 2**, we used the same microchannel structure to seed and cultivate PAO1 biofilms. An array of 52 micropatterns with 200 µm diameter

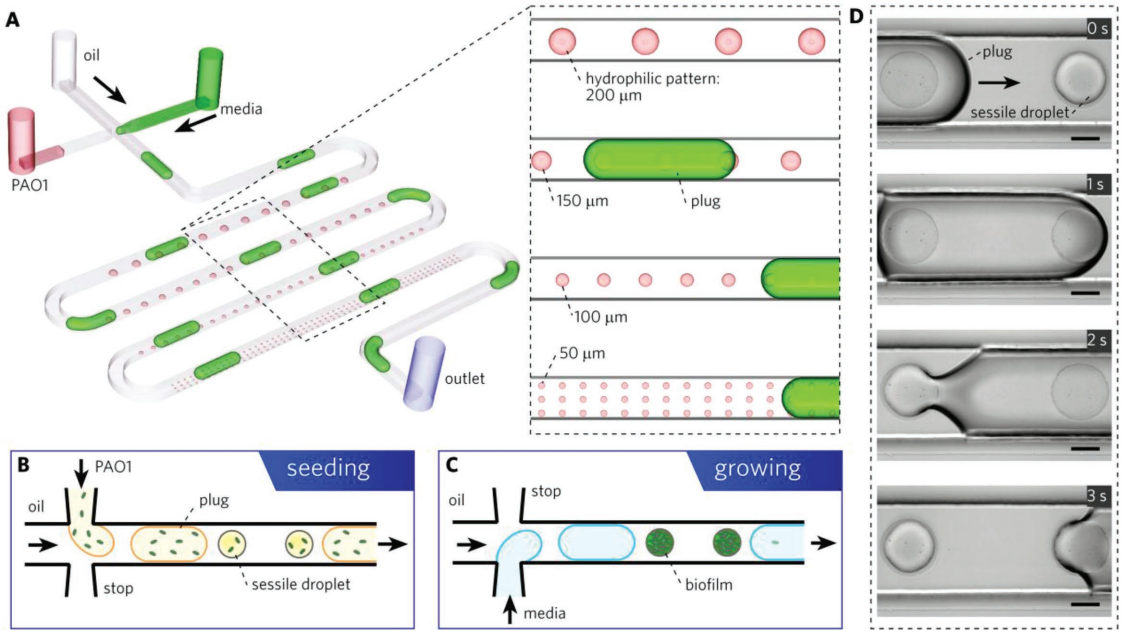

Figure 1. Grow bacterial biofilm in dynamic sessile-droplet habitats (DSH). A) 3D schematic of device with arrays of DSHs patterned on the bottom of microfluidic channel. Magnified view displays the arrangement of micropatterns. The device contains 159 of 50 µm, 27 of 100 µm, 18 of 150 µm, and 13 of 200 µm size micropatterns. B,C) Seeding and growing PAO1 biofilms in DSH device. PAO1 cells encapsulated in nanoliter droplets were infused into the continuous phase (mineral oil) using the T-junction method, and seeded on hydrophilic micropatterns under the sessile droplets. Next, flow of cell suspension was stopped, and culture medium was infused from the bottom inlet generating droplets in T-junction to supply the growth of biofilms confined within the sessile droplets. D) Time-lapse microscopic images of the fusion and splitting process between the flowing droplets and sessile droplets. The diameter of micropatterns is 200 µm. Scale bars: 100 µm.

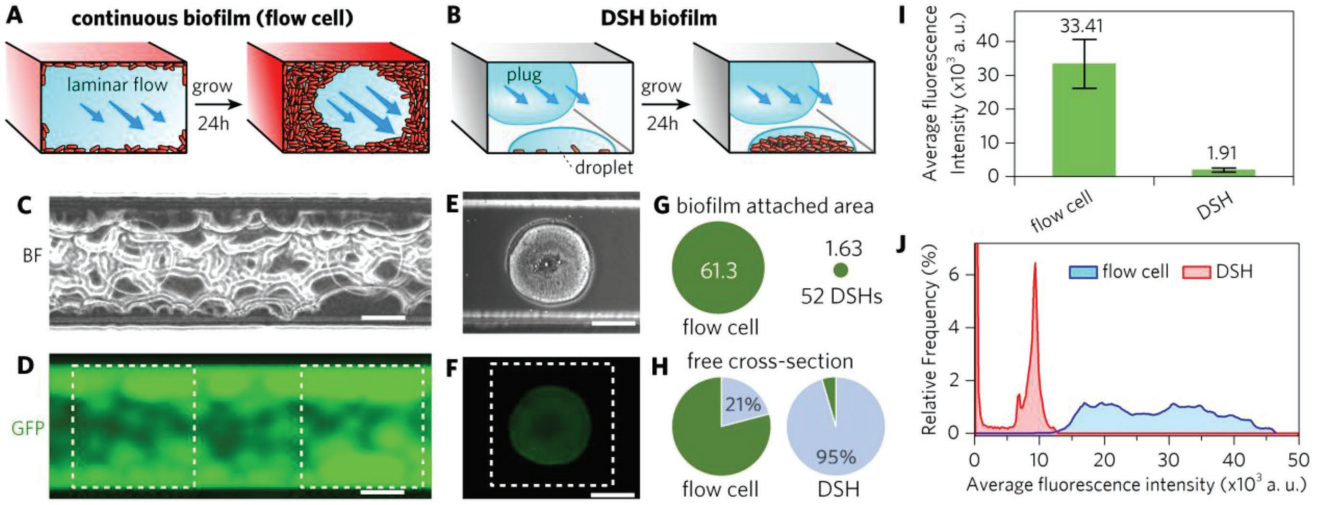

Figure 2. Comparison of biofilm formations in microfluidic flow cell and DSHs. The identical microfluidic channel design (68 mm long; 150 µm × 300 µm cross-section area) was used for both methods. 52 DSHs with diameter of 200 µm were distributed along the microfluidic channel with spacing of 600 µm. Schematic illustration of biofilm development in A) flow cell and B) DSH. C–F) Representative bright-field (BF) and green fluorescence (GFP) images for the flow cell C,D) and DSHs D,F), imaged after 24 h of seeding. Scale bars: 100 µm. G) Comparison of biofilm-attached area for flow cell and DSH. H) Estimated free cross-section at 24 h for flow cell and DSH based on fluorescence. Numbers are the areas calculated in square millimeters. I) The biomasses of biofilms evaluated by average fluorescence intensities obtained from selected regions (300 × 300 µm, as shown in panels (D) and (F)) along the microfluidic channels. Error bars, SD (flow cell, $n = 10$; DSH, $n = 24$). J) Relative frequency histograms of fluorescence images of continuous biofilm (white dashed lines in panel (D)) and DSH biofilm (white dashed line in panel (F)).

were designed for generate 52 DSH biofilms with uniform size (see the design of the device in Figure 6A). The oil flow rate of 1.0 µL min^{-1} and medium flow rate of 0.3 µL min^{-1} were used for biofilms growth in 200 µm DSHs. A flow rate of 1.3 µL min^{-1} for Luria-Bertani (LB) broth was used for continuous flow to introduce similar flow velocity. As expected, after 24 h of cultivation, the continuous biofilm (Figure 2A,C,D) covered the whole channel wall and was much denser and more heterogeneous than DSH-based biofilms (Figure 2B,E,F). Significant corner effects were observed for the continuous biofilm due to large differences between the shear stresses at the rectangular channel corners comparing with those at straight wall segments.[8] The thickness of the biofilms reached to the depth of channel (150 µm) were observed along both sides of the channel (Figure 2C,D), which resulted in dramatic increase of flow resistance and intervention along the microfluidic channel, affected the uniformity of shear force the biofilm received, and reduced the access to nutrients for the biofilms. The total biofilm attached area was 61.34 mm^2 for the continuous biofilm, compare with 1.63 mm^2 for 52 200 µm DSHs in one device (Figure 2G). As roughly estimated based on average fluorescence intensity, the overgrowth of the continuous biofilm occupied ≈79% of the cross-section of microchannel on average, leaving only ≈21% free cross-section for flow to passing through, compare with ≈95% for that of 200 µm DSHs at 24 h (Figure 2H). The estimated biomasses and relative frequency histogram of fluorescence images of the continuous flow cells and 200 µm DSHs (Figure 2I,J) also revealed that the DSH method could effectively constrain the growth of biofilms in the microfluidic channel. Therefore, the DSH method was able to provide more consistent hydrodynamic environments and avoid catastrophic disruption of flow due to exponentially fast clogging of channel.[23]

We also observed that the DSH method can significantly reduce biofilm gradients from the inlet to the outlet of the device, which normally observed in continuous reactors including microfluidic flow cells.[17] Scaling down the size of micropatterns could further decrease the biomass of biofilms on each DSH. As the volume of sessile droplets (50–200 µm in diameter, ≈0.02–1.5 nL in volume) was much smaller than the plugs (≈30 nL in volume), nutrients, and signals could be effectively exchanged with the biofilms to support its growth. Although we had not measure the exact exchange efficiency, the process which involved both convective dispersion and diffusion was likely similar to that of previous reported chemistrode devices,[20,24] which was developed for stimulate and collect chemical signals at millisecond temporal resolution. The continuous plug flow efficiently removed dispersal cells and quorum sensing signals, which also helped to eliminate possible gradient effects between neighboring DSHs. Moreover, the flow rate of the oil can be varied to apply different shear force to the biofilms and accelerate the exchanging process. An optimized oil flow rate of mineral oil of 1 µL min^{-1} was obtained based on reliable and reproducible growth of biofilms on 200 µm DSHs (Figure S4, Supporting Information).

2.3. Initializing Biofilm Growth in DSHs with Controllable Cell Numbers

At the initial stage, the irreversible attachment of bacteria to the surface was crucial for the development of biofilm.[7] The transition from reversible attachment to irreversible adhesion depended on the response of cells to the micro-environmental changes,[25] and the number of attached cells to a surface could serve as an indicator of the dynamic developmental process.[26]

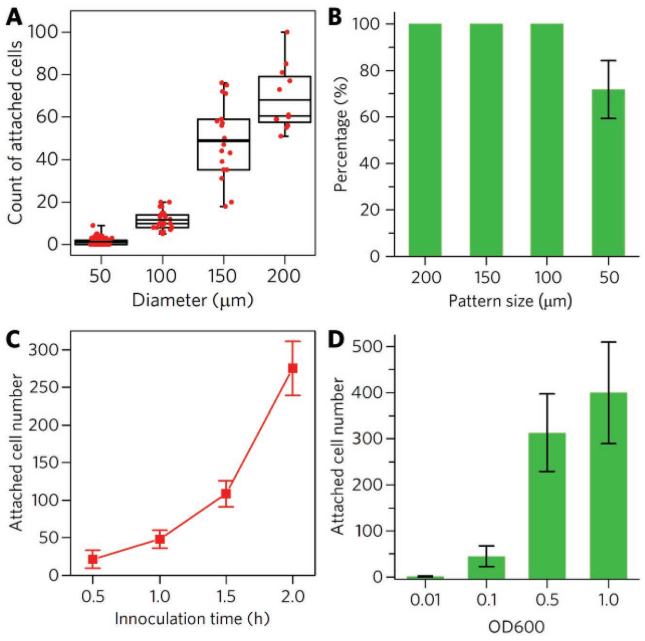

Figure 3. Attachment of PAO1 cells in DSHs for initialization of biofilm development. A) Attached cell number in DSHs with diameters of 200, 150, 100, and 50 μm after 1 h seeding with the PAO1 culture (OD600 = 0.5). B) The percentage of micropatterns with at least 1 cell attached after 1 h inoculation, with diameters from 200 to 50 μm. Error bars, SD (50 μm: $n = 159$, 100 μm: $n = 27$; 150 μm: $n = 18$; 200 μm: $n = 13$). C) The correlation of irreversibly attached PAO1 cells and seeding time on 200 μm micropatterns. Error bars represent standard deviations ($n = 26$). D) The effect of seeding cell density (OD600) on the attached cell number on 200 μm micropatterns (seeding for 2 h). Error bars, SD ($n = 13$).

To determine the specific mechanism of the effect of the area of micropatterns on the number of attached cells, we flowed PAO1 cell suspension ($OD_{600} = 0.5$) through the microchannel for 1 h to seed cells on the micropatterns with diameters of 50, 100, 150, and 200 μm, and then flowed LB broth for another 15 min to remove nonattached cells before counting cell number on each micropattern. As a result, cells only attached on the hydrophilic micropatterns throughout the microfluidic channel, and cells were distributed randomly and evenly on the array of micropatterns. The attached cell numbers varied between different micropattern sizes (**Figure 3**A; and Figure S2, Supporting Information). For DSHs with sizes of 200, 150, and 100 μm, 1 h seeding could guarantee 100% micropatterns seeded with cells (Figure 3B). However, when the diameter reduced to 50 μm, the seeding rate decreased to 71.7%, and the average attached cell number decreased to 1.43 ± 1.37 ($n = 159$).

To optimize the seeding condition, we tested seeding time from 0.5 to 2 h with PAO1 cell of $OD_{600} = 0.5$ on 200 μm micropatterns to investigate the influence of seeding time on the number of attached cells. As shown in Figure 3C, the average number of attached cells was strongly correlated to inoculation time. Next, we tested the effect of the concentration of seeding cell suspension from $OD_{600} = 0.01$ to $OD_{600} = 1.0$, with fixed seeding time of 2 h. As shown in Figure 3D, the number of attached cells varied from 1 ± 1 to 399.3 ± 110.1 ($n = 26$) on 200 μm micropatterns. And typical flow rates of inoculation plug were 1.0 μL min^{-1} for mineral oil (Q_{oil}) and 0.3 μL min^{-1} for cell suspension (Q_{cell}), which generated around 10 plugs per minute for cell attachment. To ensure the reproducibility of the afterward growth of biofilm in DSHs, $OD_{600} = 0.5$ together with an inoculation time of 2 h was selected for biofilm growth of PAO1 and its mutants.

2.4. Effect of Micropattern Size on Biofilm Development

P. aeruginosa PAO1 harbors an extraordinary ability to attach to biotic or abiotic surface through direct interaction with the surface.[27] However, when PAO1 cells were attached in a DSH with limited space, the development of biofilm might be suppressed due to constrained nutrients, shear stress, limited cell–cell interaction, and rapid diffusive loss of signaling molecules. Therefore, we assumed that micropattern size might affect the development of biofilms. To test this hypothesis, we flowed PAO1 cell suspension for 2 h to seed cells on the micropatterns with diameters from 50, 100, 150, to 200 μm. Then, LB plugs were used to supply the growth of biofilms in DSHs continuously for 24 h.

As a result, the percentage of DSHs with biofilm growth was affected by the size of micropatterns (**Figure 4**A,B). With a 2 h seeding of PAO1 cell suspension ($OD_{600} = 0.5$) at optimized condition ($Q_{cell} = 0.3$ μL min^{-1}, $Q_{oil} = 1.0$ μL min^{-1}), all DSHs with diameters of 150 and 200 μm developed biofilm after 24 h, based on the microscopic observation of significant biomass increase, and formation of multilayered structures. However, among 159 DSHs with size of 50 μm (the total area was close to that of 18 DSHs with size of 150 μm), only 12.3 DSHs (7.76%, average of three experiments) developed biofilms. By further reducing the inoculation time to 1 h, the biofilm occupation of area after 24 h incubation for DSHs with sizes of 50, 100, and 150 μm subsequently reduced to 2.5% ($n = 159$), 40.7% ($n = 27$), and 88.9% ($n = 18$), respectively, while 200 μm DSHs remained 100% ($n = 13$). For DSHs with sizes of 150 and 100 μm, 1 h seeding could guarantee 100% micropatterns seeded with PAO1 cells (Figure 3B), but not all DSHs with attached cells developed biofilms after 24 h. Interestingly, on those micropatterns with no biofilm growth, we found that cells remained attached on the surface, with negligible growth during 24 h. Thus, 200 μm was found to be a better size which could robustly develop biofilms under the current experimental settings. Collectively, these results suggested that biofilm formation was influenced by the size of attachable surface, and there existed a threshold size which attached cells may not develop into biofilms under hydrodynamic environments.

2.5. Lifespan Observation of Bacterial Biofilms under Stable Hydrodynamic Conditions

To demonstrate that the DSH method could be used to study long-term development of biofilms, two strains were applied, the wild type strain PAO1 and its Δ*psl* mutant, to cultivate their biofilms continuously for 50 h using 200 μm DSHs, with $Q_{oil} = 1$ μL min^{-1} and $Q_{media} = 0.3$ μL min^{-1}. *psl* Exopolysaccharides are key components of the biofilm matrix in *P. aeruginosa* that enable bacterial cells attachment to surface,

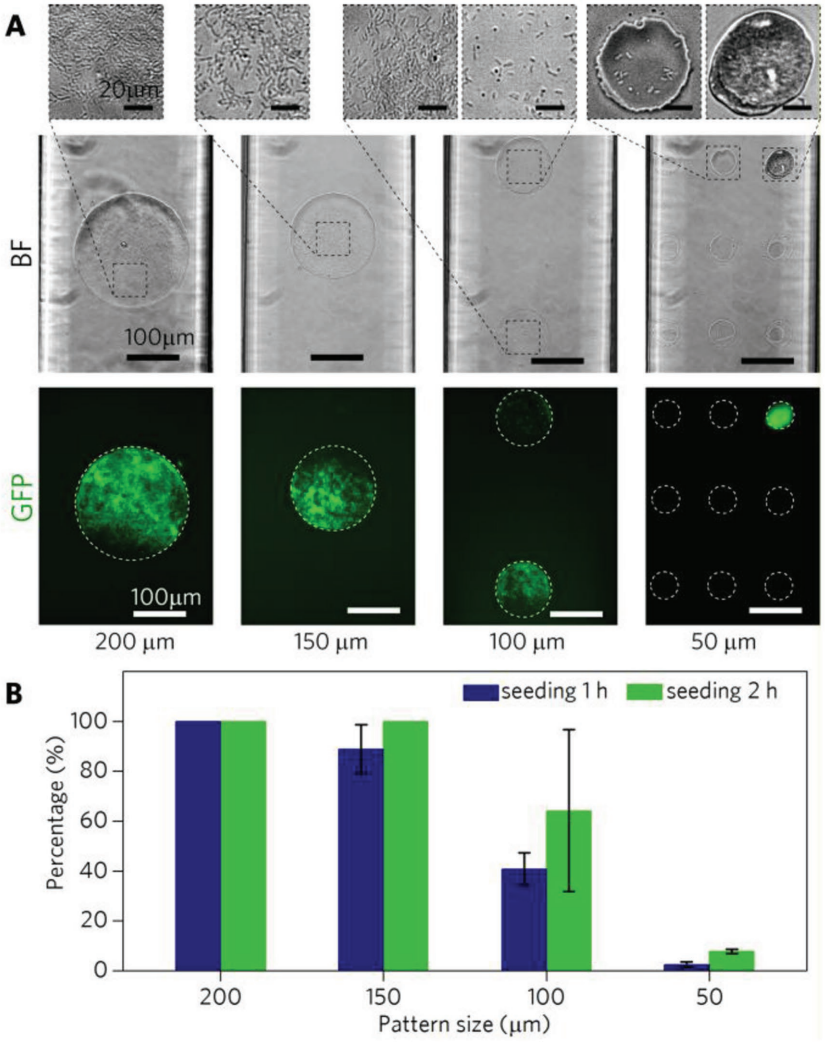

Figure 4. Biofilm formation in sessile droplets with different sizes. A) Representative microscopic images of DSH-based biofilms on micropatterns with various diameters (50, 100, 150, and 200 μm). The seeding time was 2 h, and images were acquired after 24 h growth. B) The percentages of biofilm formation in the micropatterns with different diameters. Error bars, SD (50 μm: $n = 159$, 100 μm: $n = 27$; 150 μm: $n = 18$; 200 μm: $n = 13$).

promote the bacterial cell–cell interaction, and maintain the biofilm structure. The time-series images of PAO1 and Δ*psl* biofilms demonstrated the different developmental processes (**Figure 5**A; and Videos S4–S6, Supporting Information). PAO1 exhibited robust biofilm formation on the micropatterns as its biofilms continued growing during 16 h, which began to grow out of the 200 μm size micropatterns at 24 h, and eventually formed biofilm streamers after 40 h of cultivation. In contrast, the biofilm of Δ*psl* mutant showed weak attachment on the micropatterns, reached its summit at about 22 h, and then sloughed for the first time as a plug passed by (Video S5, Supporting Information). Subsequently, we quantified the biofilm growth of both PAO1 and Δ*psl* mutant based on change of average fluorescence intensity (Figure 5B,C). For wild type PAO1, we also measured the biofilm-covered area to quantify the expansion process. We found that the development of PAO1 biofilm could be divided into three phases: the initial colonization phase (phase I), the spatially constrained growth phase (phase II), and the territorial expansion phase (phase III) (Figure 5B). The initial colonization of the micropatterns by the PAO1 biofilms lasted for about 20 h, then the biofilm biomass started to accumulate within the sessile droplets (phase II), where the growth and detachment of the cells occurred at the same time. After 32 h (phase III), biofilm biomass increased rapidly and expanded outside the micropatterns (see Video S6 recorded at 40 h, Supporting Information). The detachment ceased as the biofilm streamer became thicker and stronger. The extracellular polymeric substance (EPS) of the biofilm streamers contaminated the hydrophobic surface outside micropatterns and made them biofilm-attachable. In contrast, the Δ*psl* biofilms did not form streamers and were limited within the micropatterns, and showed obvious periodic growth and sloughing cycles which lasted for about 10–20 h (Figure 5C). To the best of our knowledge, we report for the first time of periodical growth and sloughing cycle of Δ*psl* mutant biofilms of PAO1. Collectively, these results suggested that EPS, especially *psl*, was essential for robust biofilm attachment and formation of biofilm streamers.

2.6. Antimicrobial Susceptibility Testing of PAO1 Biofilms

To determine the responses of biofilms to antibiotic exposure, we designed the device with three aqueous inlets for loading cells, culture medium, and antibiotics without cross contamination (**Figure 6**A). First, T-junction on the left was used to introduce bacterial plugs to seed PAO1 cells on an array of 200 μm DSHs for 2 h ($Q_{oil} = 1$ μL min^{-1}, $Q_{cell} = 0.3$ μL min^{-1}); second, LB medium plugs was infused from the right junction using the second aqueous inlet for 16 h at the same flow rates as the first step; third, Tob with different concentrations in LB medium was infused into the device to test its performance in biofilm eradication. As shown in Figure 6B, PAO1 biofilms exhibited exponential growth before exposure to 100 μg mL^{-1} tobramycin. The biomass decreased by 94.0% after 22 h, as determined by average fluorescent intensity of the residual biofilms (Figure 6B). As the concentration of Tob increased from 12.5 to 200 μg mL^{-1}, the eradication rate raised from 43.0% to 70.7%, while the biofilm biomass in untreated control doubled after 5 h (Figure 6C). The introduction of multiple plug generators enabled us to flexibly switch the stimulants and to dynamically record the whole process without interruption, including cell seeding, biofilm cultivation, and antimicrobial susceptibility testing.

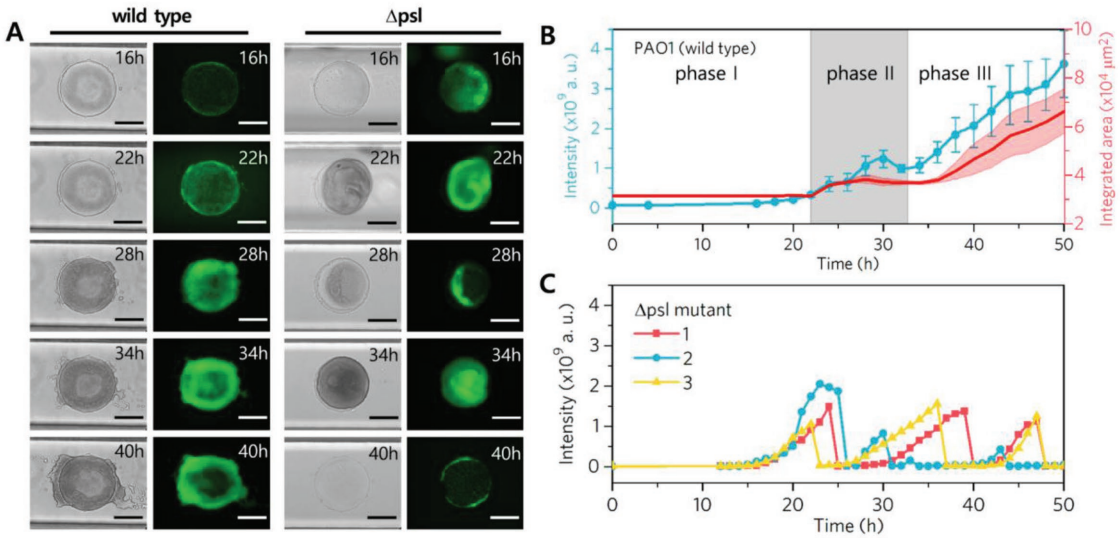

Figure 5. Lifespan observation of biofilms formed by PAO1 and its mutant. A) Time-lapse images of biofilms of PAO1 (wild type) and PAO1Δ*psl* in 200 μm size DSHs. Scale bars: 100 μm. Bright-field and fluorescence images show different growth patterns of biofilms in 40 h. B) PAO1 biofilm growth evaluated by integrated fluorescence intensity and cell covered area. Error bars, SD ($n = 13$). C) Growth of Δ*psl* biofilm in DSHs. Integrated fluorescence intensities of three representative DSHs (200 μm diameter) were drawn as red, blue, and orange plots. Flow conditions were $Q_{oil} = 1.0$ μL min^{-1}, $Q_{media} = 0.3$ μL min^{-1}.

2.7. The Roles of Flagella and Pili in the Development of Biofilms

To further demonstrate that the DSH method can quantitatively analyze both seeding and growth of biofilms, we compared the PAO1 wild type with Δ*pilA*, Δ*fliC*, and Δ*fliC*Δ*pilA* mutants on 200 μm micropatterns (**Figure 7**). We estimated the seeding performance of each strain by measuring the area occupied by the attached bacterial cells with 2 h inoculations. Biofilm growth was evaluated based on fluorescence intensity.

Type IV pili and flagella are previously reported to contribute to the biofilm initiation and development.[28,29] At the seeding stage, Δ*pilA* mutant that cannot generate functional type IV pili is weakly adhered to the surface of micropatterns, whereas the Δ*fliC* mutant that lacks flagella exhibits the highest surface adhesion among the four strains (Figure 7A,B). We founded that Δ*fliC* cells have an increased surface coverage relative to wild-type cells, which suggests that flagella may function as a swimming propeller off the surface during bacterial attachment.[30] While the attached area of Δ*fliC*Δ*pilA* is similar to wild-type PAO1. Similarly, on visual evaluation of representative biofilm images, different mutant biofilms appeared diverse on the surface. After inoculation, we grow the biofilms for 24 h by continuous feeding LB broth. The results showed that the biomass of Δ*fliC* biofilm is the highest in all four strains tested (Figure 7A,C). Collectively, these quantitative data indicate that flagella and pili not only control bacteria attachment but also biofilm structure.[30,31]

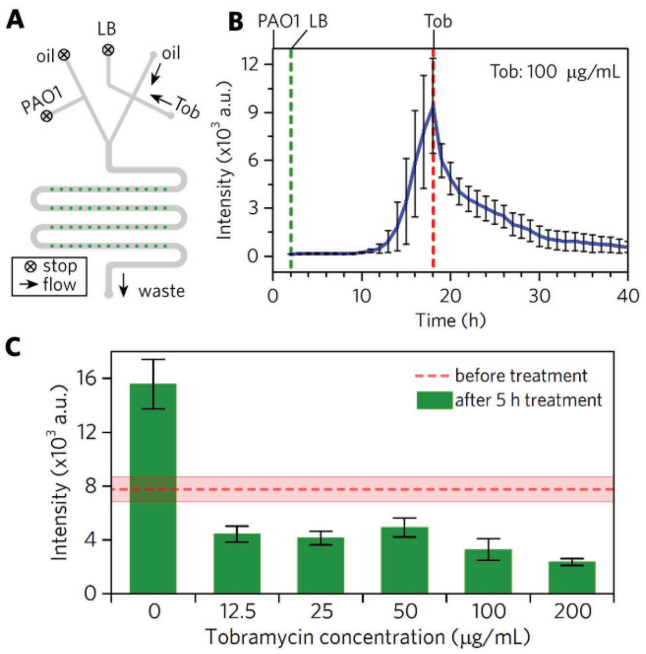

Figure 6. Antimicrobial susceptibility testing of PAO1 biofilms. A) Schematic of device with three aqueous inlets and two oil inlets for sequential introduction of cells, culture media, and antibiotic solutions. B) Temporal profile of the average fluorescence intensity of PAO1 DSHs during 18 h cultivation with LB medium and another 22 h treatment with 100 μg mL^{-1} tobramycin. C) Eradication of PAO1 biofilms by tobramycin of various concentrations after 5 h treatment. Error bars, SD ($n = 52$).

3. Conclusion

In summary, we developed a simple droplet-based method for cultivating bacterial biofilms in microfluidic channel. The device can precisely control the number of attached cells on predefined-micropatterns with different sizes, apply shear flow to study the hydrodynamic effect, analyze the growth of biofilms by time-lapse imaging, evaluate the impact of various genomic modifications, and quantify the antibiotic resistance of biofilms.

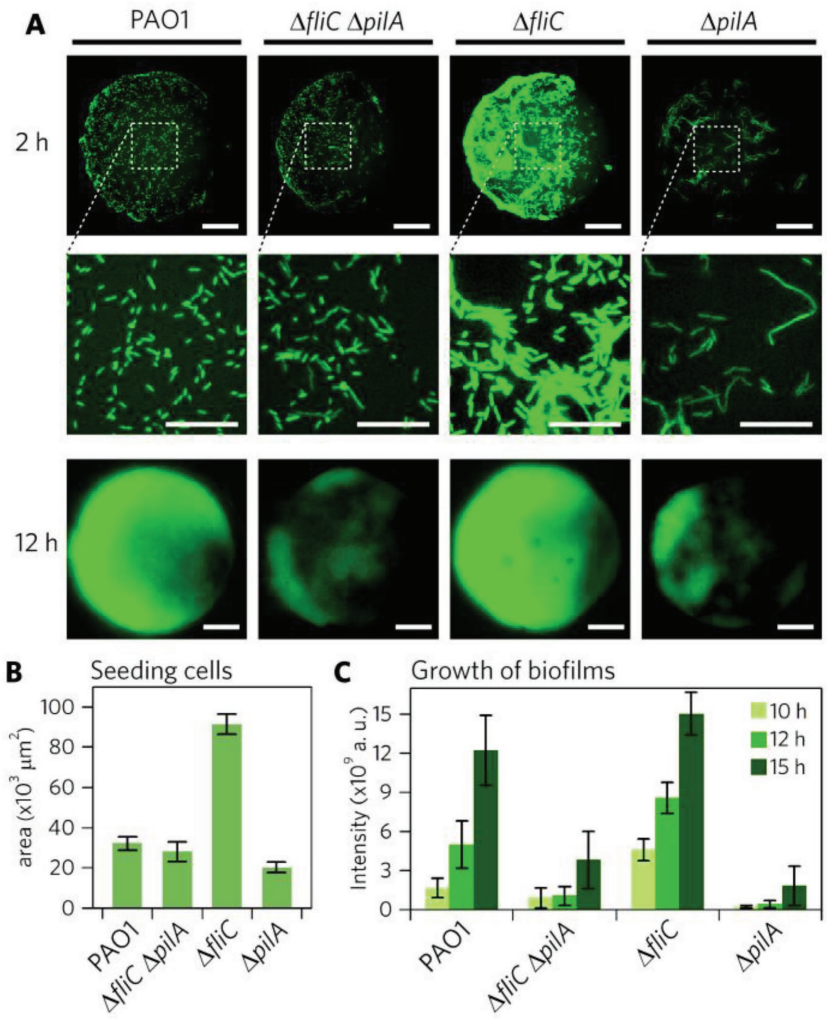

Figure 7. Quantitative analysis of the impact of flagella and pili on the development of PAO1 biofilms. A) Representative GFP microphotographs of biofilms of wild type PAO1, Δ*pilA*, Δ*fliC*, and Δ*fliC*Δ*pilA* after 2 h inoculation with zoom-in views, and growth of biofilms after 12 h cultivation. Scale bars (top to down): 50, 25, and 50 μm. B) Covering areas of attached cells were measured at 2 h. C) Biofilm total biomasses were measured at 12, 14, and 17 h. All data in (B) and (C) were obtained from the corresponding fluorescence and optical images using ImageJ software. Error bars represent standard deviations ($n = 4$). Flow conditions: $Q_{oil} = 1.0$ μL min^{-1}, $Q_{media} = 0.3$ μL min^{-1}.

Compared with continuous flow-based devices where biofilms cover all walls of the microchannel, the DSH method obtains single layer biofilms growing only on the bottom of the channel with precisely defined area and boundary. Different nanoliter plugs can be flexibly switched, adjusted, or stopped during the experiment for programmable and periodical chemical and hydrodynamic stimulations of biofilms, with significant reduction of the consumption of culture media compare with continuous flow cells. This method had led to interesting observations of area-dependency of biofilm growth, periodical sloughing of biofilms under shear flow, territory expansion of biofilms, and formation of biofilm streamers, which in turn proved the DSH biofilms hold the intrinsic properties of biofilms previously observed in flow cell devices and in nature.

We believe that this simple and versatile DSH method can be commonly applied in more quantitative studies of bacterial biofilms, especially for development and aging of biofilms under shear stress and spatial confinements, shedding light on better understandings of bacterial biofilms in clinical and environmental settings. The predictable and persistent hydrodynamic environments provided by the DSH method is especially suitable for long-term studies of microbial biofilms. Moreover, the sessile droplet approach may be extended in various biological applications ranging from the growth, differentiation, and proliferation of adherent mammalian cells to tissue engineering.

4. Experimental Section

The experimental setup is shown in Figure 1. In brief, the microfluidic device contains two layers, top PDMS layer with microchannels and the bottom glass plate with hydrophilic/hydrophobic hybrid patterns (see the detailed fabrication process in Figure S1, Supporting Information). The carrier oil was mineral oil without surfactant. The channel was prefilled with mineral oil before loading of bacterial suspension. Aqueous plugs were formed as described previously.[32,33] The hydrophilic micropatterns were first seeded with bacterial cell plugs, followed by continuous infusion of culture media plugs for long-term cultivation. The number of attached cells, as well as the dynamic growth of biofilms in DSHs were determined by fluorescence imaging under an inverted microscope. See the Supporting Information for more detailed procedures.

Supporting Information

Supporting Information is available from the Wiley Online Library or from the author.

Acknowledgements

This study was supported by China Ocean Mineral Resources R&D Association (No. DY135-B-02), the National Natural Science Foundation of China (Nos. 31470221 and 31570126), National Key Research and Development Program of China (Nos. 2016YFC0100900 and 2016YFE0205800), Beijing Municipal Science & Technology Commission (No. Z161100000116042), the National Basic Research Program of China (No. 973 Program 2014CB846002), the Strategic Priority Research Program of Chinese Academy of Sciences (No. XDB15040102), the Key Program of Frontier Sciences of Chinese Academy of Sciences (No. QYZDB-SSW-SMC008), the Key Research Program of the Chinese Academy of Sciences (No. KFZD-SW-219-4), and Science and Technology Service Network Initiative (STS) of Chinese Academy of Sciences (No. KFJ-SW-STS-165).

Conflict of Interest

The authors declare no conflict of interest.

Keywords

antibiotic resistance, biofilms, microfluidics, micropatterns, sessile droplets

Received: February 16, 2018
Revised: March 10, 2018
Published online: May 2, 2018

[1] L. Hall-Stoodley, J. W. Costerton, P. Stoodley, *Nat. Rev. Microbiol.* **2004**, *2*, 95.
[2] T. J. Battin, L. A. Kaplan, J. D. Newbold, C. Hansen, *Nature* **2003**, *426*, 439.
[3] H. C. Flemming, J. Wingender, *Nat. Rev. Microbiol.* **2010**, *8*, 623.
[4] D. Davies, *Nat. Rev. Drug Discovery* **2003**, *2*, 114.
[5] P. E. Kolenbrander, R. J. Palmer, S. Periasamy, N. S. Jakubovics, *Nat. Rev. Microbiol.* **2010**, *8*, 471.
[6] W. M. de Vos, *NPJ Biofilms Microbiomes* **2015**, *1*, 15005.
[7] J. Azeredo, N. F. Azevedo, R. Briandet, N. Cerca, T. Coenye, A. R. Costa, M. Desvaux, G. Di Bonaventura, M. Hebraud, Z. Jaglic, M. Kacaniova, S. Knochel, A. Lourenco, F. Mergulhao, R. L. Meyer, G. Nychas, M. Simoes, O. Tresse, C. Sternberg, *Crit. Rev. Microbiol.* **2017**, *43*, 313.
[8] N. B. Aznaveh, M. Safdar, G. Wolfaardt, J. Greener, *Lab Chip* **2014**, *14*, 2666.
[9] M. Salta, L. Capretto, D. Carugo, J. A. Wharton, K. R. Stokes, *Biomicrofluidics* **2013**, *7*, 064118.
[10] K. P. Kim, Y. G. Kim, C. H. Choi, H. E. Kim, S. H. Lee, *Lab Chip* **2010**, *10*, 3296.
[11] J. Deng, A. Dhummakupt, P. C. Samson, J. P. Wikswo, L. M. Shor, *Anal. Chem.* **2013**, *85*, 5411.
[12] L. Richter, C. Stepper, A. Mak, A. Reinthaler, R. Heer, M. Kast, H. Bruckl, P. Ertl, *Lab Chip* **2007**, *7*, 1723.
[13] C. B. Chang, J. N. Wilking, S. Kim, H. C. Shum, D. A. Weitz, *Small* **2015**, *11*, 3954.
[14] S. Yu, T. Su, H. Wu, S. Liu, D. Wang, T. Zhao, Z. Jin, DuW , M. J. Zhu, S. L. Chua, L. Yang, D. Zhu, L. Gu, L. Z. Ma, *Cell Res.* **2015**, *25*, 1352.
[15] A. Karimi, D. Karig, A. Kumar, A. M. Ardekani, *Lab Chip* **2015**, *15*, 23.
[16] J. Kim, H. S. Kim, S. Han, J. Y. Lee, J. E. Oh, S. Chung, H. D. Park, *Lab Chip* **2013**, *13*, 1846.
[17] M. K. Kim, F. Ingremeau, A. Zhao, B. L. Bassler, H. A. Stone, *Nat. Microbiol.* **2016**, *1*, 15005.
[18] J. H. Lee, J. B. Kaplan, W. Y. Lee, *Biomed. Microdevices* **2008**, *10*, 489.
[19] C. Y. Jiang, L. Dong, J. K. Zhao, X. Hu, C. Shen, Y. Qiao, X. Zhang, Y. Wang, R. F. Ismagilov, S. J. Liu, W. Du, *Appl. Environ. Microbiol.* **2016**, *82*, 2210.
[20] D. Chen, W. Du, Y. Liu, W. Liu, A. Kuznetsov, F. E. Mendez, L. H. Philipson, R. F. Ismagilov, *Proc. Natl. Acad. Sci. USA* **2008**, *105*, 16843.
[21] Y. Liu, R. F. Ismagilov, *Langmuir* **2009**, *25*, 2854.
[22] J. C. McDonald, G. M. Whitesides, *Acc. Chem. Res.* **2002**, *35*, 491.
[23] K. Drescher, Y. Shen, B. L. Bassler, H. A. Stone, *Proc. Natl. Acad. Sci. USA* **2013**, *110*, 4345.
[24] D. Chen, W. Du, R. F. Ismagilov, *New J. Phys.* **2009**, *11*, 075017.
[25] M. D. Hoffman, L. I. Zucker, P. J. Brown, D. T. Kysela, Y. V. Brun, S. C. Jacobson, *Anal. Chem.* **2015**, *87*, 12032.
[26] P. Stoodley, K. Sauer, D. G. Davies, J. W. Costerton, *Annu. Rev. Microbiol.* **2002**, *56*, 187.
[27] K. Sauer, A. K. Camper, G. D. Ehrlich, J. W. Costerton, D. G. Davies, *J. Bacteriol.* **2002**, *184*, 1140.
[28] L. Ma, K. D. Jackson, R. M. Landry, M. R. Parsek, D. J. Wozniak, *J. Bacteriol.* **2006**, *188*, 8213.
[29] S. Wang, M. R. Parsek, D. J. Wozniak, L. Z. Ma, *Environ. Microbiol.* **2013**, *15*, 2238.
[30] M. Klausen, A. Heydorn, P. Ragas, L. Lambertsen, A. Aaes-Jorgensen, S. Molin, T. Tolker-Nielsen, *Mol. Microbiol.* **2003**, *48*, 1511.
[31] K. B. Barken, S. J. Pamp, L. Yang, M. Gjermansen, J. J. Bertrand, M. Klausen, M. Givskov, C. B. Whitchurch, J. N. Engel, T. Tolker-Nielsen, *Environ. Microbiol.* **2008**, *10*, 2331.
[32] L. Li, D. Mustafi, Q. Fu, V. Tereshko, D. L. L. Chen, J. D. Tice, R. F. Ismagilov, *Proc. Natl. Acad. Sci. USA* **2006**, *103*, 19243.
[33] L. Dong, D. W. Chen, S. J. Liu, W. Du, *Sci. Rep.* **2016**, *6*, 24192.